



Article

Sensitivity of the 4–10-Day Planetary Wave Structures in the Middle Atmosphere to the Solar Activity Effects in the Thermosphere

Andrey V. Koval^{1,2,*} , Nikolai M. Gavrilov¹, Ksenia A. Didenko^{1,2}, Tatiana S. Ermakova^{1,2} 
and Elena N. Savenkova²

¹ Atmospheric Physics Department, Saint Petersburg State University, 198504 Saint-Petersburg, Russia

² Satellite Oceanography Laboratory, Russian State Hydrometeorological University, 192007 Saint-Petersburg, Russia

* Correspondence: a.v.koval@spbu.ru

Abstract: Numerical simulation of the general atmospheric circulation was performed to estimate changes in amplitudes of the westward-travelling planetary waves (PWs) at altitudes from the Earth's surface up to 300 km under different solar activity (SA) levels. The three-dimensional nonlinear mechanistic model of circulation of the middle and upper atmosphere "MUAM" was used. The atmospheric general circulation and PW amplitudes were calculated based on ensembles containing 16 model runs for conditions corresponding to low and high SA. PWs having periods of 4–10 days were considered. Comparison with the data of digital ionosondes showed that the MUAM model is capable of reproducing the considered PW modes at thermospheric heights. It is shown that under high SA conditions, PW amplitudes are significantly larger in the thermosphere and smaller in the middle atmosphere. The observed PW structures are influenced not only by changes in atmospheric refractive index and Eliassen–Palm flux but also by varying PW reflection in the lower thermosphere, which can change proportions of the wave energy transferred from the lower atmosphere to the upper layers and reflected downwards.

Keywords: numerical modeling; planetary waves; solar activity; atmospheric dynamics; MUAM



Citation: Koval, A.V.; Gavrilov, N.M.; Didenko, K.A.; Ermakova, T.S.; Savenkova, E.N. Sensitivity of the 4–10-Day Planetary Wave Structures in the Middle Atmosphere to the Solar Activity Effects in the Thermosphere. *Atmosphere* **2022**, *13*, 1325. <https://doi.org/10.3390/atmos13081325>

Academic Editors: Alexei Krivolutsky and Anna Kukoleva

Received: 13 July 2022

Accepted: 17 August 2022

Published: 19 August 2022

Publisher's Note: MDPI stays neutral with regard to jurisdictional claims in published maps and institutional affiliations.



Copyright: © 2022 by the authors. Licensee MDPI, Basel, Switzerland. This article is an open access article distributed under the terms and conditions of the Creative Commons Attribution (CC BY) license (<https://creativecommons.org/licenses/by/4.0/>).

1. Introduction

Currently, numerical modeling can be considered as the most powerful tool for studying the interaction of various atmospheric processes and their relative contribution to the formation of the dynamic and temperature regime of the atmosphere. For instance, modeling allows one to produce "idealized" studies of certain processes, rectified from superimposing other extreme events, which could exist in experimental data.

It is widely known that planetary waves (PWs) with the same or similar periods regularly coexist in the middle atmosphere and upper thermosphere/ionosphere (e.g., [1,2]). Borries and Hoffmann [3] showed the existence of strong planetary-wave-type oscillations in the ionosphere by analyzing the maps of total electron content. They found that characteristics of standing and propagating waves in the ionosphere are similar to stratospheric PWs. At the same time, Laštovicka [4] assumed that planetary waves could propagate from the middle atmosphere to altitudes of more than 130–140 km only indirectly, through secondary PW excitation by dissipating PW-modulated tides [5,6], or through vertical plasma drifts [7].

Conditions of PW generation and propagation may depend on cyclic changes in the solar activity (SA). The incoming solar radiation and heating depend on the SA, which undergoes cyclic changes with a period of about 11 years (see e.g., [8]). In the study [9], it was shown that SA changes in the thermosphere can significantly influence middle-atmosphere

circulation and amplitudes of quasi-stationary PWs. Wave reflection in the lower thermosphere may also influence the circulation of the middle atmosphere (e.g., [9,10]). Among the reasons for PW reflection at thermospheric heights can be significant temperature and wind gradients. A study of influence of SA changes on the structures of the westward-propagating PWs was recently performed by Koval and co-authors [11]. It was shown that changes in the zonal wind and temperature caused by solar activity variations can modify amplitudes of PWs in the thermosphere by up to 100%. However, the authors failed to obtain statistically significant data on changes in the PW amplitudes in the middle atmosphere. In the current study, we expanded the scope of ensemble model simulations and used a new approach to statistical data processing. In addition, we compared the PW spectra simulated in the thermosphere with observational data.

Most of the numerical models used to estimate the propagation and reflection of PWs in the thermosphere have their upper boundaries at altitudes of about 120–150 km. In the current study, we observed changes in atmospheric circulation using the middle- and upper-atmosphere model “MUAM”, which allows performing numerical simulation of the general circulation and PWs in the atmosphere at altitudes from the Earth’s surface up to about 300 km.

2. Methodology

In order to study dynamic processes in the atmosphere and simulate the general atmospheric circulation, the 3-dimensional nonlinear mechanistic numerical model of the general circulation of the middle and upper atmosphere “MUAM” [12,13] was used. It is based on the original COMMA model developed at the University of Cologne, Germany [14]. The horizontal grid steps of the model are 5.625° in longitude and 5° in latitude. The vertical grid of the model has 56 nodes as a log-isobaric coordinate $z = -H \times \ln(p/p_0)$, where p_0 is the surface pressure and H is pressure scale height.

The radiative block of the MUAM takes into account the dependence of solar radiation on SA. The main indicator of SA is the solar radio flux at the wavelength of 10.7 cm (F10.7). The F10.7 flux changes during the 11-year solar activity cycle (e.g., [15]). According to analysis of F10.7 observations during the last six solar cycles (Royal Observatory of Belgium, [16]), the values of F10.7 = 70, 130, 220 sfu (1 sfu = 10^{-22} W/(m²Hz)) were chosen, which characterized low, medium and high SA levels, respectively. To take into account the effects of ionospheric charged particles on the neutral gas motion for different SA levels, the contribution of the electromagnetic Lorentz force was added to the equations of motion for the horizontal components of the wind speed. This force depends on ionospheric conductivities, which were calculated for different SA levels using the IRI-Plus ionospheric model [17] and the NRLMSISE-00 model of the neutral atmosphere [18] and implemented into the MUAM with the method proposed in [19]. A detailed description of the processes taken into account in the current version of the model and the scheme of a numerical experiment can be found in [9].

The MUAM model can reproduce stationary planetary waves and atmospheric normal modes (NMs) [20]. At low boundary, stationary PW amplitudes are calculated from the geopotential heights in the lower atmosphere obtained from the stratospheric assimilation dataset JRA-55 [21]. The MUAM involves NM parameterization, which uses additional terms in the heat balance equation, having a form of time-dependent sinusoidal components with zonal wavenumbers $m = 1$ or $m = 2$ and periods matching to the simulated NMs. For setting the latitude structures of NM components, the parameterization uses respective Hough functions, obtained with the method described in [22]. Periods of NMs are equal to the resonant periods of atmospheric reaction to the wave forcing at low boundary. In the current study, NMs (1,1), (1,2), (1,3), (2,1) and (2,2), according to the classification proposed by Longuet-Higgins [23], which have periods of about 5, 10, 16, 4 and 7 days, respectively, are observed. The NM sources used in the MUAM provide amplitudes of simulated NM comparable with the observed ones in the stratosphere [24]. Here, it is necessary to make a remark: a part of the PW turned out to be outside the scope of the study. For example,

a hot topic in the aeronomy community is that of 6-day waves, discussed in detail by Gan et al. [25]. Furthermore, quasi-two-day waves and eastward-propagating equatorially trapped Kelvin waves are subjects for further analyses.

To study the thermospheric effects of changes in SA (in its pure form, without taking into account variations in direct solar irradiance on the middle atmosphere) on the circulation and PWs in the middle atmosphere, we specified SA changes in the MUAM only at altitudes higher than 100 km (similar to [9]). To improve statistical significance of the results achieved, 16 pairs of the MUAM runs for low and high SA were performed. The initial and background conditions in all MUAM runs were the same. The difference in MUAM runs was the shift in the phases of stratospheric vacillations between PWs and the mean wind [26]. Initial perturbations together with PW phases are controlled in the MUAM by the model day of inclusion of daily variations in solar heating in the course of the initialization, which varies between 120 and 135 with the step of 1 day in the simulated ensemble of the MUAM runs. For the PW calculation, the modelled temporal interval between the middle of December and the end of February was extracted. Averaging over 16 model runs and over two months allowed us to achieve 95% statistical significance and diminish effects of extreme atmospheric processes such as sudden stratospheric warming events, which occur in individual MUAM runs. The statistical processing of the ensemble results based on Student's *t*-test is described by Koval [27].

3. Results and Discussion

To verify the ability of the MUAM to reproduce PWs at thermospheric heights, the results of simulations were compared with the observational data obtained with the DPS-4 ionosonde at Saint Petersburg. The DPS-4 ionosonde measures the signatures of electromagnetic waves reflected from ionospheric free electrons. Using multiparameter ionograms, the ionosonde reconstructs the real-time data on the properties of the ionosphere and electron concentration profiles. Typically, the ionosonde scans frequencies from 1 MHz to 20 MHz, transmitting modulated HF radio waves and then receiving and analyzing the echo reflected from the ionosphere. The total electron content and other ionospheric characteristics are calculated from the critical plasma frequency data. Detailed characteristics are described in [28] and on the website of the Center for Atmospheric Research, Lowell University, USA: <https://ulcar.uml.edu/digisonde.html> (accessed on 1 June 2021).

Methods of the ionosonde data analysis were described by Gavrilov and Koval [29]. In the present study, we used the results of spectral analysis using the standard method of Lomb–Scargle [30,31]. The method is based on the approximation of unequally spaced measured values of the analyzed quantities by harmonic functions with different frequencies. In comparison with the standard software based on the Lomb–Scargle method, the algorithm used in the present study made it possible to also determine amplitudes and phases of all spectral components. According to data from the DPS-4 digital ionosonde operating at the Peterhof campus of Saint Petersburg State University (59.88° N, 29.82° E), the spectra of the critical frequency of the F2 ionospheric layer, f_0F_2 , were calculated for 60-day time intervals corresponding to different seasons in order to detect PWs at ionospheric heights.

For the purpose of comparative analysis of observational and computational data, we calculated the spectra of model fluctuations in the temperature of the thermosphere at an altitude of 200 km at the grid node of the MUAM, corresponding to the geographical location of the ionosonde in Peterhof. The spectra were obtained by applying the approach described above for the ionosondes data.

Figure 1 shows the spectrum of the critical frequency f_0F_2 in Peterhof (left) obtained for a 60-day time interval, centered on 31 January 2019, and the corresponding spectrum of temperature fluctuations according to the MUAM data (right). In this case, we are interested in the spectrum peaks at close frequencies, which could indicate that the MUAM may reproduce PW oscillations observed in the ionosphere. In particular, when comparing the left and right panels of Figure 1, one can see the presence of similar peaks corresponding to the semidiurnal and diurnal tides and to 4-, 5-, 6-, 7-, 10- and 16-day PWs, as well as an

oscillation with a period of about 30 days. Figure 1 also demonstrates some differences between measured and modeled PW spectra. The reason for the differences may be a contribution of PW-type oscillations generated in the ionosphere, which are not involved in the MUAM simulations of the temperature variations in the neutral component.

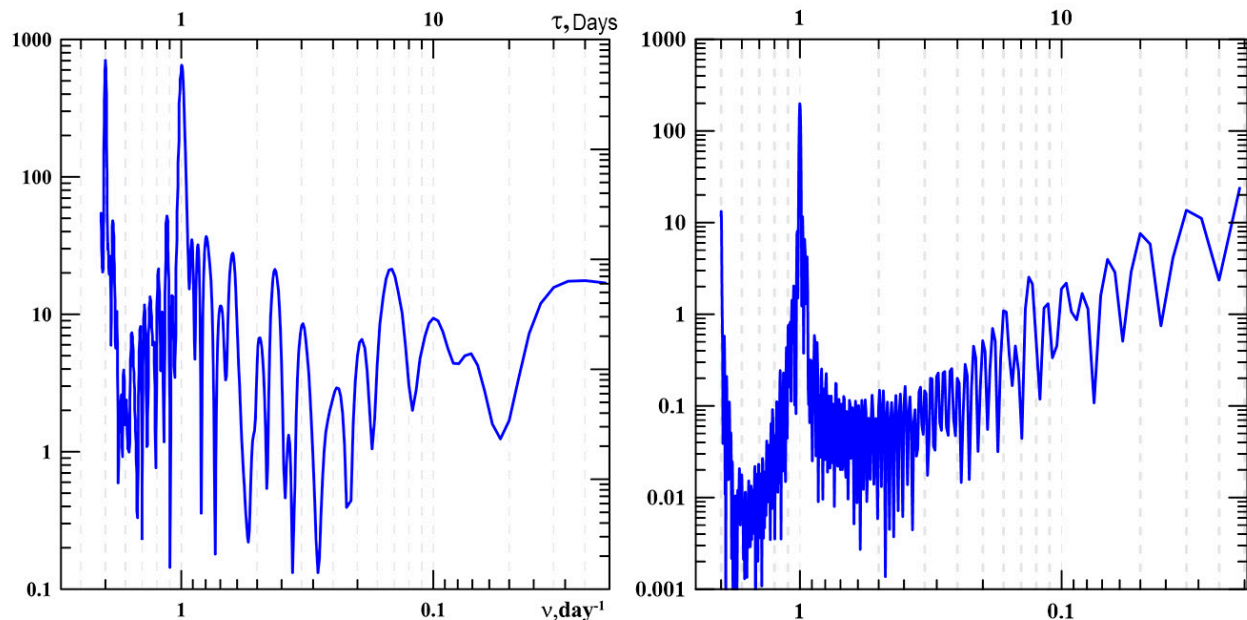


Figure 1. The spectrum of the critical frequency f_0F_2 in Peterhof in a sliding 60-day time interval, centered on 31 January 2019 (left), and the corresponding spectrum of temperature fluctuations at an altitude of 200 km according to the MUAM model data (right). The lower axis is the frequency (1/day), and the upper axis is the period in days.

Geopotential height variations due to PWs. In order to calculate PW amplitudes and obtain their statistically significant changes in the middle atmosphere, from each of the 16 MUAM runs, the same temporal interval between the middle of December and the end of February was extracted. This interval was divided into five 15-day subintervals. For each subinterval, amplitudes and phases of PW modes were estimated. To study SA influence, for each of 16 pairs of the MUAM runs for high and low SA, the differences between PW amplitudes at each grid point were obtained and averaged over the altitude–latitude cluster containing 9 adjacent grid points. In this way, 720 individual differences (16 runs \times 5 subintervals \times 9 grid points) were observed. Using this approach, we obtained statistically significant nonzero differences at 95% significance level between the mean values of PW amplitudes under high and low SA at almost all altitudes.

Figure 2 reveals simulated latitude–height distributions of PW amplitudes under high SA, as well as their differences due to SA changes in the thermosphere. One can see that the main maximums of 7- and 10-day PWs exist at the middle and high latitudes of the Northern (winter) Hemisphere. Amplitudes of 4- and 5-day waves also have maximums in the Southern (summer) Hemisphere. This can be connected with their higher westward phase speeds. According to Charney and Drazin [32], PWs propagate upward only in the regions where the difference between the zonal wind and wave phase speed is positive. Differences in PW amplitudes between high and low levels of SA are shown in the right panels of Figure 2. Respective differences in the zonal-mean velocity and temperature fields caused by changes from high to low SA can be found in Figure 4 of the study by Koval et al. [9]. Changes in the general circulation modify spatial distributions of PW amplitudes. Under high SA, PW amplitudes are generally (up to 100%) smaller at thermospheric heights, compared to low SA. The most significant decrease at high SA can be seen at heights above 200 km. The eastward direction of atmospheric circulation during the winter season in

the middle atmosphere of the Northern Hemisphere contributes to better propagation of planetary waves. At middle and high latitudes of the Southern Hemisphere, the largest negative differences can be seen in the right panel of Figure 2b at altitudes above 150 km.

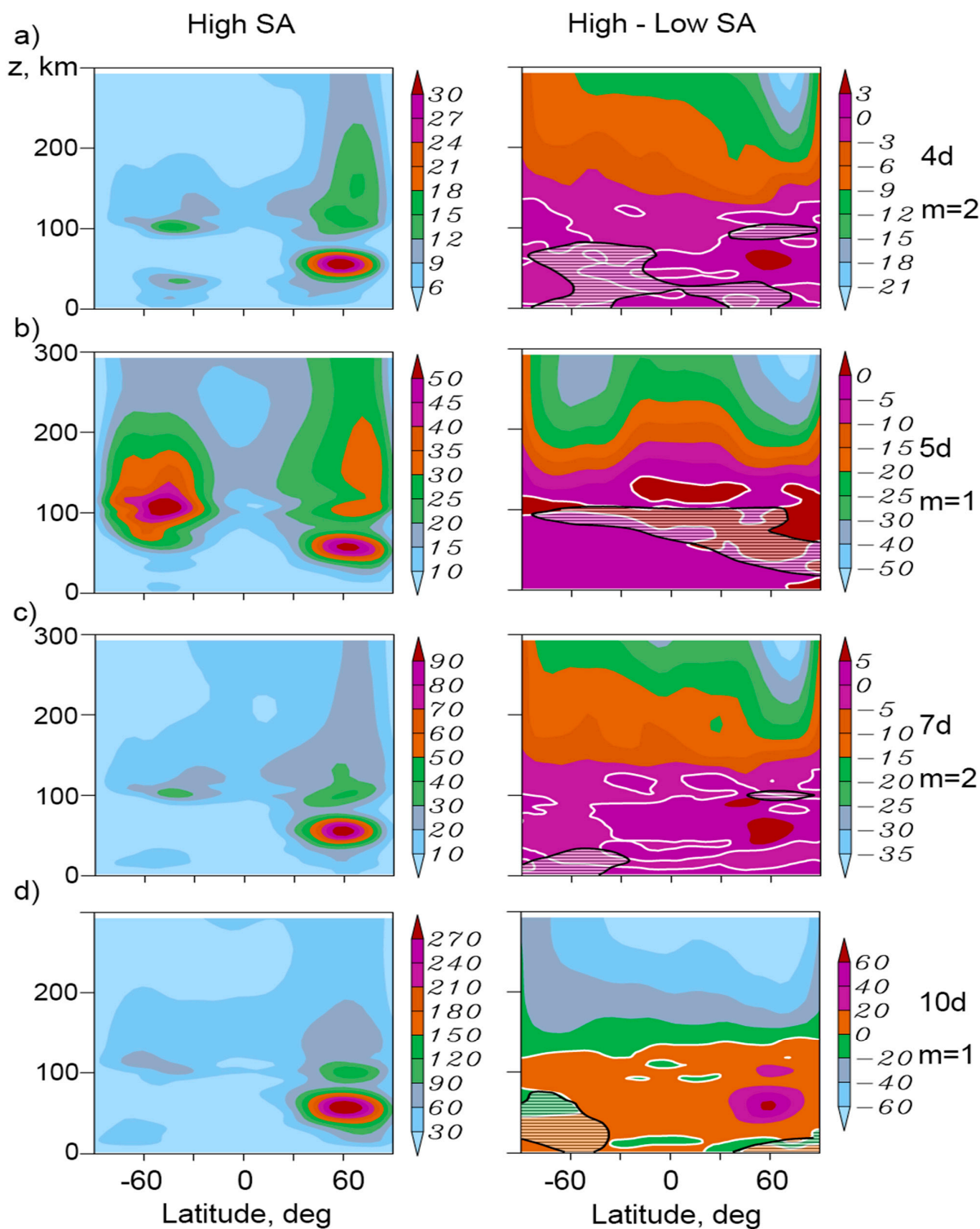


Figure 2. Amplitudes of the geopotential height variations (in gp.m.) caused by the westward-travelling PWs having periods 4, 5, 7 and 10 days ((a–d), respectively) under high SA (left) and differences (right) due to SA changes in thermosphere, averaged over 16-member ensembles and from mid-December–February. Areas shaded with lines show statistically unconfident differences. Altitude range 0–300 km.

Magnitudes and the structure of simulated 5-day and 10-day PWs are in general agreement with those obtained from TIMED/SABER temperature measurements at altitudes of the middle atmosphere, mesosphere and lower thermosphere [33–35]. The existence of the simulated PW modes with the same periods at ionospheric heights was confirmed by many observations of the total electron content at different latitudes (e.g., [36,37]). In the middle atmosphere, the amplitudes of the observed PWs were also successfully compared with those calculated on the basis of geopotential height fields from the reanalysis of meteorological information MERRA-2 [38].

Figure 3 reproduces Figure 2 but for altitude range 0–100 km. At altitudes below 100 km, the right panels demonstrate mainly positive differences corresponding to larger PW amplitudes under high SA at the middle northern latitudes. However, amplitude differences in the middle atmosphere are much smaller than in the thermosphere: they range from 10–15% for 4–7-day PW, and for the 10-day PW, the maximum is 25%, as shown in Figure 3d.

The refractivity index (n^2) and Eliassen–Palm flux (EP flux) were calculated for the waves shown in Figure 2 to interpret the obtained PW differences. The theory of planetary waves [39] predicts waveguides in the regions of positive n^2 , while EP-flux vectors reflect direction of enhancement of the wave activity. Our calculations show that in most cases, wider waveguides and upward-directed increments of EP-flux under high SA correspond to positive changes in PW amplitudes in the northern stratosphere–mesosphere.

All of the considered PW modes have in general larger amplitudes in the northern middle atmosphere under high SA than under low SA, while at the same time, changes in PW amplitudes in the thermosphere are mainly opposite. These changes may be associated with amplification of partial reflection of upward-propagating waves downward from the lower thermosphere under high SA. Similar effect was previously discussed by Lu et al. and Koval et al. [9,10]. Consideration of refractivity index reveals regions of increased n^2 at altitudes of 100–130 km at middle and high latitudes of the Northern Hemisphere. Increased vertical gradients of n^2 in these regions may produce increasing partial reflection of PWs propagating from the lower atmospheric layers. Our assumption of the wave reflection is confirmed by the fact that the EP fluxes in the northern lower thermosphere are directed downwards. This PW partial reflection can change proportion based on wave energy, reflecting downwards and propagating to the thermosphere.

Increased vertical temperature gradients and Brunt–Väisälä frequency in the lower thermosphere under high SA can also lead to partial reflections of PWs propagating from below [40,41]. Temperature gradients and partial reflection should be stronger at high SA, which can contribute to a smaller proportion of PW energy penetrating to the thermosphere and to smaller PW amplitudes in the thermosphere at high SA, as shown in Figures 2 and 3.

Phases of the PWs were also analyzed. Strong phase shifts exist at altitudes of 80–100 km for 5- and 10-day PWs having the zonal wavenumber 1, especially at low SA. This can be connected with possible influence of plasma drift on PW propagation into the lower ionosphere and on the wave phases [4]. Temporal time lag in PWs propagating into the lower ionosphere of up to several days was found by Pancheva et al. [42] and by Stray and Espy [43].

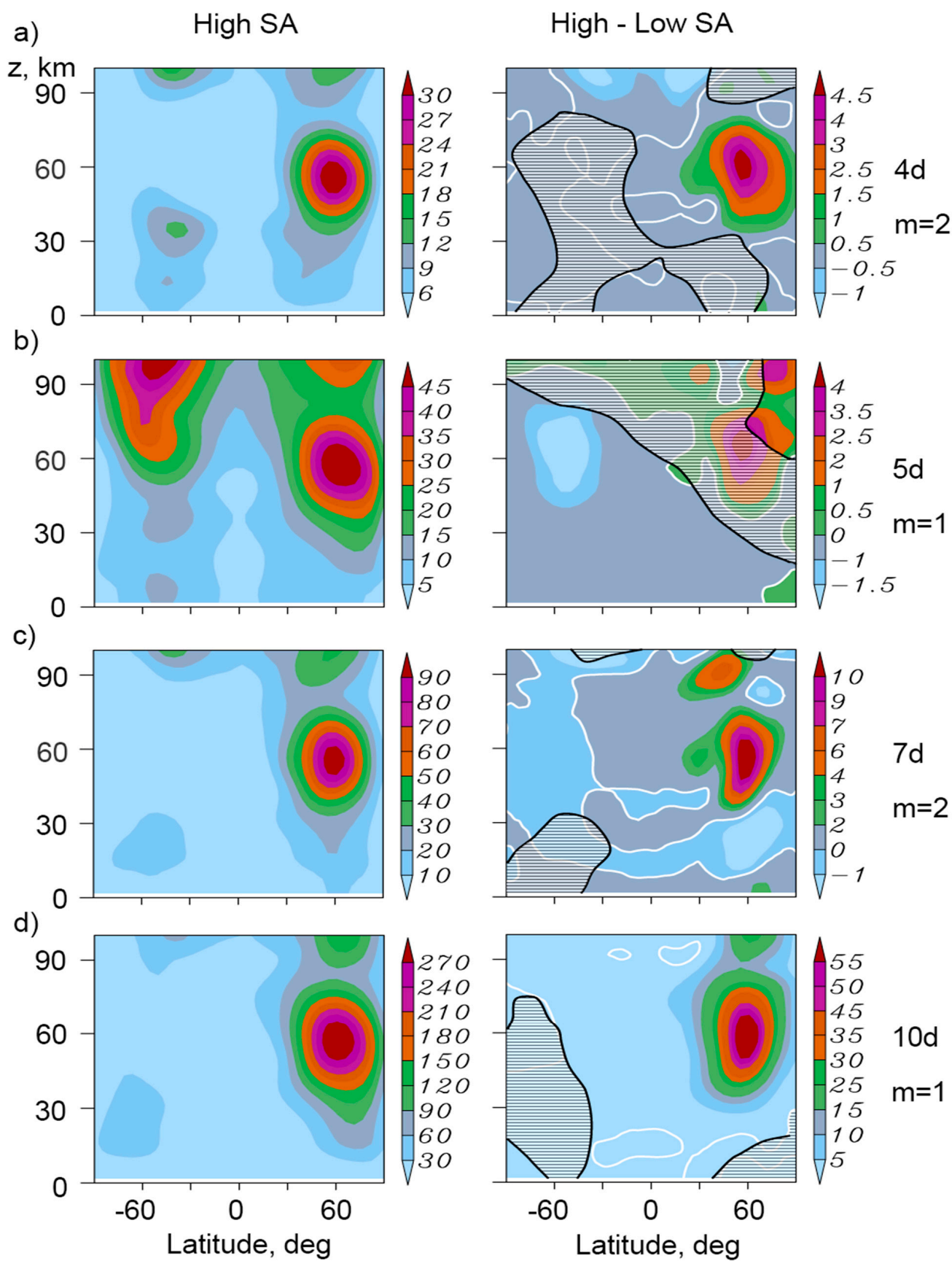


Figure 3. The same as Figure 2 but for altitude range 0–100 km.

4. Conclusions

The features of propagation of the westward-travelling PWs from the Earth's surface to the altitude of 300 km at different levels of solar activity (SA) were studied. Only the thermospheric influence was investigated, determined mainly by changes in UV radiation, while changes in the direct effects of solar radiation on the middle atmosphere at different SA levels were not taken into account. The model of the middle and upper atmosphere MUAM was used, in which different SA levels were set at altitudes of more than 100 km. Below 100 km, the same conditions for all experiments were set corresponding to the medium level of solar activity. Two 16-member ensembles of model simulations corresponding to high and low SA were observed.

Comparison of the spectra of temperature fluctuations in the thermosphere at individual grid nodes of the MUAM model with fluctuations of the critical frequency f_0F_2 according to the data from digital ionosondes DPS-4 was performed. It was shown that the model reproduces observed fluctuations in the thermosphere corresponding to semidiurnal and diurnal tides, as well as to 4-, 5-, 6-, 7-, 10- and 16-day PWs. A comparison of the waves calculated in the hydrodynamic fields of the MUAM with the data of satellite observations and the data of reanalysis of meteorological information also showed a good correspondence between the observed and simulated PW structures.

Statistically significant results were obtained illustrating the effects of SA changes in the thermosphere on the PW amplitudes in the middle atmosphere. At thermospheric altitudes, PW amplitudes are smaller under high SA, which is explained by the narrowing of their waveguides and weakening of the EP fluxes. Taking into account the SA changes in the thermosphere leads to statistically significant changes in the PW amplitudes in the middle atmosphere, which can reach 10–15%.

Since the PWs propagate from the lower atmosphere, in addition to the refractive index and the EP flux structure, their propagation is significantly influenced by the partial reflection of the PWs at the heights of the lower thermosphere. This reflection is caused by a change in vertical temperature gradients. Different reflections of the PW can contribute to a change in the proportions of the PW wave energy penetrating into the thermosphere and reflecting backwards and to a change in the PW amplitudes both in the thermosphere and in the middle atmosphere.

Author Contributions: All authors made valuable contributions in writing and editing of the text, data analysis and visualization of the results. A.V.K. and N.M.G.: conceptualization, numerical modeling; K.A.D.: statistical processing; T.S.E. and E.N.S.: ionosonde data processing and visualization. All authors have read and agreed to the published version of the manuscript.

Funding: Adjustment of the MUAM for different SA levels, ensemble simulations and analyses of the atmospheric circulation and statistical processing were supported by the Russian Science Foundation (grant 20-77-10006). Calculation of PW structures up to the thermosphere and comparing the modeled data with observations were supported by the Ministry of Science and High Education of the Russian Federation (agreement 075-15-2021-583).

Data Availability Statement: In accordance with the statement 1296 of the Civil Code of the Russian Federation, the Russian State Hydrometeorological University (RSHU) has all rights on the MUAM code. To access and use the computer codes one should obtain a permission from the Rector of RSHU via the address 79, Voronezhskaya street, St. Petersburg, Russia, 192007, phone: 007 (812) 372-50-92. The authors can assist in obtaining the permission. The data of analyzed modeling can be freely accessed upon request from Andrey Koval (a.v.koval@spbu.ru).

Conflicts of Interest: The authors declare no conflict of interest.

References

1. Chang, L.C.; Liu, J.Y.; Palo, S.E. Propagating planetary wave coupling in SABER MLT temperatures and GPS TEC during the 2005/2006 austral summer. *J. Geophys. Res.* **2011**, *116*, A10324. [[CrossRef](#)]
2. Pancheva, D.; Mukhtarov, P. Planetary wave coupling of the atmosphere–ionosphere system during the Northern winter of 2008/2009. *Adv. Space Res.* **2012**, *50*, 1189–1203. [[CrossRef](#)]

3. Borries, C.; Hoffmann, P. Characteristics of F2-layer planetary wave-type oscillations in northern middle and high latitudes during 2002 to 2008. *J. Geophys. Res. Space Phys.* **2010**, *115*, A00G10. [CrossRef]
4. Laštovicka, J. Forcing of the ionosphere by waves from below. *J. Atmos. Sol. Terr. Phys.* **2006**, *68*, 479–497. [CrossRef]
5. Meyer, C.K. Gravity wave interactions with mesospheric planetary waves: A mechanism for penetration into the thermosphere-ionosphere system. *J. Geophys. Res.* **1999**, *104*, 28181–28196. [CrossRef]
6. Yamazaki, Y.; Richmond, A.D. A theory of ionospheric response to upward-propagating tides: Electrodynamical effects and tidal mixing effects. *J. Geophys. Res. Space Phys.* **2013**, *118*, 5891–5905. [CrossRef]
7. Liu, H.L.; Richmond, A.D. Attribution of ionospheric vertical plasma drift perturbations to large-scale waves and the difference on solar activity. *J. Geophys. Res. Space Phys.* **2013**, *108*, 2452–2465. [CrossRef]
8. Hathaway, D.H. The Solar Cycle. *Living Rev. Sol. Phys.* **2010**, *7*, 15. [CrossRef]
9. Koval, A.V.; Gavrilov, N.M.; Pogoreltsev, A.I.; Shevchuk, N.O. Reactions of the middle atmosphere circulation and stationary planetary waves on the solar activity effects in the thermosphere. *J. Geophys. Res. Space Phys.* **2019**, *124*, 10645–10658. [CrossRef]
10. Lu, H.; Scaife, A.A.; Marshall, G.J.; Turner, J.; Gray, L.J. Downward wave reflection as a mechanism for the stratosphere-troposphere response to the 11-year solar cycle. *J. Clim.* **2017**, *30*, 2395–2414. [CrossRef]
11. Koval, A.V.; Gavrilov, N.M.; Pogoreltsev, A.I.; Shevchuk, N.O. Influence of solar activity on penetration of traveling planetary-scale waves from the troposphere into the thermosphere. *J. Geophys. Res. Space Phys.* **2018**, *123*, 6888–6903. [CrossRef]
12. Pogoreltsev, A.I.; Vlasov, A.A.; Fröhlich, K.; Jacobi, C. Planetary waves in coupling the lower and upper atmosphere. *J. Atmos. Sol. Terr. Phys.* **2007**, *69*, 2083–2101. [CrossRef]
13. Pogoreltsev, A.I. Generation of normal atmospheric modes by stratospheric vacillations. *Izv. Atmos. Ocean. Phys.* **2007**, *43*, 423–435. [CrossRef]
14. Ebel, A.; Berger, U.; Krueger, B.C. Numerical simulations with COMMA, a global model of the middle atmosphere. *SIMPO Newsl.* **1995**, *12*, 22–32.
15. Tapping, K.F. Recent solar radio astronomy at centimeter wavelength: The temporal variability of the 10.7 cm flux. *J. Geophys. Res.* **1987**, *92*, 829–838. [CrossRef]
16. Royal Observatory of Belgium (ROB). 2013. Available online: <http://sidc.be/silso/datafiles> (accessed on 18 November 2017).
17. Gulyaeva, T.L.; Huang, X.; Reinisch, B.W. Ionosphere-plasmasphere model software for ISO. *Acta Geod. Geophys. Hung.* **2002**, *37*, 143–152. [CrossRef]
18. Picone, J.M.; Hedin, A.E.; Drob, D.P.; Aikin, A.C. NRLMSISE-00 empirical model of the atmosphere: Statistical comparisons and scientific issues. *J. Geophys. Res. Space Phys.* **2002**, *107*, 1468. [CrossRef]
19. Shevchuk, N.O.; Ortikov, M.Y.; Pogoreltsev, A.I. Modeling of atmospheric tides with account of diurnal variations of ionospheric conductivity. *Russ. J. Phys. Chem. B* **2018**, *12*, 576–589. [CrossRef]
20. Pogoreltsev, A.I.; Savenkova, E.N.; Pertsev, N.N. Sudden stratospheric warmings: The role of normal atmospheric modes. *Geomagn. Aeron.* **2014**, *54*, 357–372. [CrossRef]
21. Kobayashi, S.; Ota, Y.; Harada, H. The JRA-55 Reanalysis: General Specifications and Basic Characteristics. *J. Meteorol. Soc. Jpn.* **2015**, *93*, 5–48. [CrossRef]
22. Swartztrauber, P.N.; Kasahara, A. The vector harmonic analysis of Laplace’s tidal equations. *SIAM J. Sci. Stat. Comp.* **1985**, *6*, 464–491. [CrossRef]
23. Longuet-Higgins, M.S. The eigenfunctions of Laplace’s tidal equation over a sphere. *Philos. Trans. R. Soc. Lond.* **1968**, *262*, 511–607. [CrossRef]
24. Pogoreltsev, A.I.; Kanukhina, A.Y.; Suvorova, E.V.; Savenkova, E.N. Variability of Planetary Waves as a Signature of Possible Climatic Changes. *J. Atmos. Sol.-Terr. Phys.* **2009**, *71*, 1529–1539. [CrossRef]
25. Gan, Q.; Wang, W.; Yue, J.; Liu, H.; Chang, L.C.; Zhang, S.; Burns, A.; Du, J. Numerical simulation of the 6 day wave effects on the ionosphere: Dynamo modulation. *J. Geophys. Res. Space Phys.* **2016**, *121*, 10–103. [CrossRef]
26. Holton, J.R.; Mass, C. Stratospheric vacillation cycles. *J. Atmos. Sci.* **1976**, *33*, 2218–2225. [CrossRef]
27. Koval, A.V. Statistically significant estimates of influence of solar activity on planetary waves in the middle atmosphere of the Northern Hemisphere as derived from MUAM model data. *Sol. Terr. Phys.* **2019**, *5*, 53–59. [CrossRef]
28. Reinisch, B.W.; Paznukhov, V.V.; Galkin, I.A.; Altadill, D.; McElroy, J. Advancing Digisonde Technology: The DPS-4D. Radio Sounding and Plasma Physics. American Institute of Physics. *AIP Conf. Proc.* **2008**, *974*, 127–143.
29. Gavrilov, N.M.; Koval, A.V. Spectra of tides and planetary waves from the data of ionosonde measurements near Saint Petersburg. In Proceedings of the 27th International Symposium on Atmospheric and Ocean Optics, Atmospheric Physics, Moscow, Russia, 5–9 July 2021; Volume 119167, pp. 1645–1649. [CrossRef]
30. Lomb, N. Least-squares frequency analysis of unequally spaced data. *Astrophys. Space Sci.* **1976**, *39*, 447–462. [CrossRef]
31. Scargle, J.D. Statistical aspects of spectral analysis of unevenly spaced data. *Astrophys. J.* **1982**, *263 Pt 1*, 835–853. [CrossRef]
32. Charney, J.G.; Drazin, P.G. Propagation of planetary-scale disturbances from the lower into the upper atmosphere. *J. Geophys. Res.* **1961**, *66*, 83–109. [CrossRef]
33. Pancheva, D.; Mukhtarov, P.; Andonov, B.; Forbes, J.M. Global distribution and climatological features of the 5–6-day planetary waves seen in the SABER/TIMED temperatures (2002–2007). *J. Atmos. Sol.-Terr. Phys.* **2010**, *72*, 26–37. [CrossRef]

34. Riggin, D.M.; Liu, H.-L.; Lieberman, R.S.; Roble, R.G.; Russell, J.M., III; Mertens, C.J.; Mlynczak, M.G.; Pancheva, D.; Franke, S.J.; Murayama, Y.; et al. Observations of the 5-day wave in the mesosphere and lower thermosphere. *J. Atmos. Sol.-Terr. Phys.* **2013**, *68*, 323–339. [[CrossRef](#)]
35. Forbes, J.M.; Zhang, X. Quasi-10-day wave in the atmosphere. *J. Geophys. Res.* **2015**, *120*, 11079–11089. [[CrossRef](#)]
36. Borries, C.; Jakowski, N.; Jacobi, C.; Hoffmann, P.; Pogoreltsev, A.I. Spectral analysis of planetary waves seen in ionospheric total electron content (TEC): First results using GPS differential TEC and stratospheric reanalyses. *J. Atmos. Sol.-Terr. Phys.* **2007**, *69*, 2442–2451. [[CrossRef](#)]
37. Pedatella, N.M.; Forbes, J.M. Modulation of the equatorial F-region by the quasi-16-day planetary wave. *Geophys. Res. Lett.* **2009**, *36*, L09105. [[CrossRef](#)]
38. Gelaro, R.; McCarty, W.; Suárez, M.J.; Todling, R.; Molod, A.; Takacs, L.; Randles, C.A.; Darmenov, A.; Bosilovich, M.G.; Reichle, R.; et al. The Modern-Era Retrospective Analysis for Research and Applications, version 2 (MERRA-2). *J. Clim.* **2017**, *30*, 5419–5454. [[CrossRef](#)]
39. Andrews, D.G.; Holton, J.R.; Leovy, C.B. *Middle Atmosphere Dynamics*; Academic Press: New York, NY, USA, 1987; p. 489.
40. Geller, M.A.; Alpert, J.C. Planetary wave coupling between the troposphere and the middle atmosphere as a possible Sun-weather mechanism. *J. Atmos. Sci.* **1980**, *37*, 1197–1215. [[CrossRef](#)]
41. Arnold, N.F.; Robinson, T.R. Solar cycle changes to planetary wave propagation and their influence on the middle atmosphere circulation. *Ann. Geophys.* **1998**, *16*, 69–76. [[CrossRef](#)]
42. Pancheva, D.; Alberca, L.F.; Morena, B.A. Simultaneous observations of quasi-two-day variations in the lower and upper ionosphere over Europe. *J. Atmos. Sol.-Terr. Phys.* **1994**, *56*, 43–50. [[CrossRef](#)]
43. Stray, N.H.; Espy, P.J. Planetary wave-like oscillations in the ionosphere retrieved with a longitudinal chain of ionosondes at high northern latitudes. *J. Atmos. Sol.-Terr. Phys.* **2018**, *171*, 225–233. [[CrossRef](#)]